


## Interplay of charge ordering and superconductivity in two-dimensional $2H$ group V transition-metal dichalcogenides

Chao-Sheng Lian <sup>\*</sup>*School of Physics and Microelectronics, Zhengzhou University, Zhengzhou 450001, China*

(Received 10 November 2022; revised 15 January 2023; accepted 20 January 2023; published 31 January 2023)

Layered  $2H-TX_2$  with  $T = \text{Nb, Ta}$  and  $X = \text{S, Se}$  exhibit rich dimensionality effects on charge density wave (CDW) order and superconductivity, but comprehensive understanding of these correlated quantum phases in the two-dimensional limit of  $2H-TX_2$  is still lacking, hindering their practical applications. Here, I calculate from first principles the phonon linewidth and bare susceptibility to study the origin of CDW formation in  $\text{NbSe}_2$ ,  $\text{TaS}_2$ ,  $\text{TaSe}_2$ , and  $\text{NbS}_2$  monolayers, analyze their relative CDW strength, and evaluate electron-phonon superconductivity within the fully anisotropic Migdal-Eliashberg theory. A peaked linewidth of the longitudinal acoustic branch and no Fermi-surface nesting around  $\mathbf{q}_{\text{CDW}}$  indicate CDW instability driven by the wave-vector-dependent electron-phonon coupling. The  $3 \times 3$  CDW ground state favors a distinct hollow-centered clustering of transition-metal atoms, with larger distortion amplitude in  $\text{NbSe}_2$  and  $\text{TaSe}_2$  than in  $\text{TaS}_2$  and  $\text{NbS}_2$ . Superconducting results of the monolayer CDW phase prove that strong spin-orbit coupling effects are dominant in determining the critical temperature  $T_c$  of each system via modifying both the strength and anisotropic extent of electron-phonon interactions. I also recapitulate measured opposite thickness dependencies of  $T_c$  in  $\text{NbX}_2$  and  $\text{TaX}_2$ , and show that whether superconductivity is weakened or enhanced in monolayer limit relies on specific evolution of CDW-modulated Fermi-level density of states and electron-phonon matrix elements under reduced dimensionality. This work lays the foundation for applications of  $2H$  group V transition-metal dichalcogenides in versatile nanoscale quantum devices.

DOI: [10.1103/PhysRevB.107.045431](https://doi.org/10.1103/PhysRevB.107.045431)

### I. INTRODUCTION

The interplay and control of many-body collective orders in low-dimensional materials is a vital and alluring research topic in condensed matter physics [1,2]. Metallic layered transition-metal dichalcogenides (TMDs)  $TX_2$  with  $T = \text{Ti, V, Zr, Nb, Ta}$  and  $X = \text{S, Se, Te}$  have been intensively studied for their varied charge-density waves (CDWs), superconductivity, and Mott insulating state. Of particular interest are the  $2H$  group V TMDs showing intrinsic coexistence of CDW and superconducting states without applying doping, intercalation, or pressure [3,4]. This uniqueness makes  $2H-TX_2$  a promising platform for exploring the pure dimensionality effects on interactions between the two quantum states and tuning them in a cleaner way compared to chemical modifications. Initial data in the bulk [5–9] pointed to their mutually exclusive interaction, as when the CDW is enhanced with rising transition temperature from 33 (0) K in  $2H\text{-NbSe}_2$  ( $2H\text{-NbS}_2$ ) to 75 (120) K in  $2H\text{-TaS}_2$  ( $2H\text{-TaSe}_2$ ), the superconducting critical temperature  $T_c$  decreases from 7 (5.7) K in  $2H\text{-NbSe}_2$  ( $2H\text{-NbS}_2$ ) down to 0.8 (0.1) K in  $2H\text{-TaS}_2$  ( $2H\text{-TaSe}_2$ ). A competing relation also occurs in pressurized  $2H\text{-NbSe}_2$  with slightly increased  $T_c$  upon CDW disappearance [10,11], but in pressurized  $2H\text{-TaS}_2$  and  $2H\text{-TaSe}_2$   $T_c$  substantially increases up to 9 K within a robust CDW phase [12], implying that competition between CDW and superconductivity may not be universally applicable. In

this context, the dimensionality modifications of different electronic phases in atomically thin  $2H-TX_2$ -based devices revealed by recent experiments (hereafter  $1H-TX_2$  denotes the monolayer analog of  $2H-TX_2$ ) need to be more closely examined.

In metallic TMDs, the behavior of CDW in the two-dimensional (2D) limit [13–21] can be rather complicated: while reduced dimensionality favors a stronger CDW by reinforcing nesting-driven Peierls instabilities or electron-phonon interactions, larger fluctuation effects tend to impair long-range CDW coherence. Bulk experiments [22–25] suggest electron-phonon coupling (EPC) as the major driving force of CDW, as opposed to Fermi-surface nesting or saddle-point singularities, but the mechanism triggering the CDW phase in 2D limit is still unclear. Exfoliated monolayers for  $1H\text{-NbSe}_2$  ( $1H\text{-TaSe}_2$ ) were found to exhibit a strongly enhanced (slightly weakened) CDW compared to the bulk [13,14], in contrast to the trend of CDW reported in corresponding epitaxial monolayers [15,16]. For  $1H\text{-NbS}_2$  ( $1H\text{-TaS}_2$ ), though the exfoliated monolayers show no Raman (electrical) CDW signature [14,17], CDW ordering emerges (persists) in epitaxially grown samples based on scanning tunneling measurements [18,19]. Such controversies imply the CDW formation in monolayer  $1H-TX_2$  is susceptible to sample disorder and environment, raising the issue of what behavior on earth their intrinsic CDW order follows.

Concerning the evolution of superconductivity, existing data [26–34] revealed gradually decreasing (increasing)  $T_c$  in  $2H\text{-NbSe}_2$  and  $2H\text{-NbS}_2$  ( $2H\text{-TaS}_2$  and  $2H\text{-TaSe}_2$ ) with declining thickness. At present, the role of spin-orbit interactions

<sup>\*</sup>cslian@zzu.edu.cn

in different  $2H-TX_2$  and how CDW electronic modulation impacts their superconducting order in reduced dimensions are less understood. In particular, the physical origins of the observed opposite  $T_c$  trends in 2D  $NbX_2$  and  $TaX_2$  systems remain unsettled.

In this work, I present comprehensive theoretical studies on the mechanism of CDW, electron-phonon superconductivity, and interplay of CDW and superconducting orders in 2D limit of  $2H$  group V TMDs. For all monolayer  $1H-TX_2$ , prominent peaking of the linewidth of the longitudinal acoustic (LA) phonon branch and no Fermi-surface nesting in the electronic susceptibility around  $\mathbf{q}_{CDW}$  unveil a CDW driven by momentum-dependent EPC. I unveil their common  $3 \times 3$  CDW structure with a hollow-centered clustering of transition-metal atoms, showing greater distortion amplitude in  $NbSe_2$  and  $TaSe_2$  than in  $TaS_2$  and  $NbS_2$ . Electron-phonon superconducting calculations of the monolayer CDW phase highlight the effects of spin-orbit interactions on the detailed EPC properties and critical temperature  $T_c$ . By examining the change in CDW electronic structure from bulk to monolayer  $TX_2$ , a strengthened CDW is revealed, but whether this impairs or boosts superconductivity depends on the competition between CDW-modulated Fermi-level density of states (DOS) and reinforced electron-phonon matrix elements in 2D limit.

## II. METHODOLOGY

All calculations are performed using the QUANTUM ESPRESSO package [35] with the Perdew-Burke-Ernzerhof generalized gradient approximation [36] for the exchange-correlation interaction. I employ relativistic norm-conserving pseudopotentials [37,38] to include the effects of spin-orbit coupling (SOC) on both the electronic structure and lattice dynamics. A vacuum of 12 Å is used for modeling  $1H-TX_2$  monolayer, and van der Waals interaction in the bulk is treated by the DFT-D3 method [39]. A plane-wave cutoff energy of 50 (70) Ry and a Methfessel-Paxton smearing [40] of 0.01 (0.005) Ry are adopted for  $TaX_2$  ( $NbX_2$ ) systems. All geometries including both the normal and CDW phases are optimized until the remanent atomic forces are less than  $10^{-4}$  Ry/Å. For the  $3 \times 3$  CDW phase of monolayer  $1H-TX_2$ , the dynamical matrices and the linear variation of the self-consistent potential are computed within density functional perturbation theory [41] with a  $6 \times 6$   $\mathbf{k}$  mesh and a  $3 \times 3$   $\mathbf{q}$  mesh, and electron-phonon matrix elements are interpolated [42,43] onto  $60 \times 60$   $\mathbf{k}$ -point and  $30 \times 30$   $\mathbf{q}$ -point grids. The anisotropic Migdal-Eliashberg theory as implemented in the EPW code [43–45] with a Matsubara frequency cutoff of 0.4 eV and delta smearings of 12.5–37.5 meV (electrons) and 0.05 meV (phonons) is used to calculate the superconducting gap and critical temperature. For the normal (CDW) phase of bulk  $2H-TX_2$ , a  $54 \times 54 \times 18$  ( $12 \times 12 \times 10$ )  $\mathbf{k}$  mesh is used for evaluating the electronic DOS.

## III. RESULTS AND DISCUSSION

### A. Mechanism of CDW instability in $1H-TX_2$

I first investigate the lattice dynamics and electronic susceptibility to clarify the CDW formation in  $1H-TX_2$  monolayers, whose  $1 \times 1$  normal phase has a honeycomb lattice

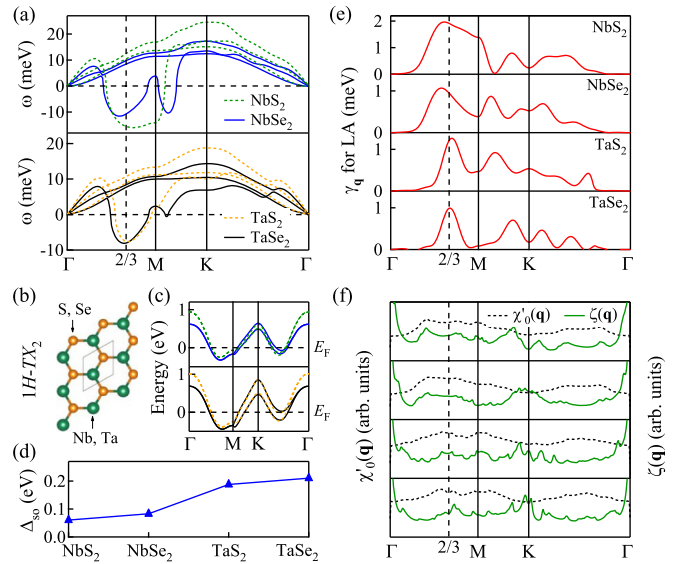


FIG. 1. (a) Phonon instability of monolayer  $1H-TX_2$  in trigonal prismatic structure, as depicted in (b). (c) Electronic band structure of  $1H-TX_2$  [referring to line styles in (a) for different systems] around the Fermi level ( $E_F$ ). (d) The Fermi-surface average for  $\mathbf{k}$ -dependent spin-orbit splitting in the half-filled  $d$  band,  $\Delta_{SO}$  of 0.061 eV ( $NbS_2$ ), 0.083 eV ( $NbSe_2$ ), 0.188 eV ( $TaS_2$ ), and 0.21 eV ( $TaSe_2$ ). (e) Phonon linewidth  $\gamma_q$  of the soft LA branch. (f) Real part of the bare electronic susceptibility  $\chi'_0(\mathbf{q})$  and Fermi-surface nesting function  $\zeta(\mathbf{q})$ . All results are calculated with the inclusion of SOC.

with transition-metal  $T$  atoms sandwiched between chalcogen  $X$  atoms in a trigonal prismatic structure [Fig. 1(b)]. The calculated phonon spectra with SOC in Fig. 1(a) show that, for all considered  $TX_2$  systems ( $T = Nb, Ta$  and  $X = S, Se$ ), the LA phonon branch softens along  $\Gamma M$  yielding marked instability around wave vector  $\mathbf{q}_{CDW} = \frac{2}{3}\Gamma M$ . For  $1H-NbSe_2$ , the most unstable phonon mode appears at  $\mathbf{q} = 0.59\Gamma M$ , while for  $1H-TaS_2$  and  $1H-TaSe_2$ , it is localized almost exactly at  $\mathbf{q} = \frac{2}{3}\Gamma M$ . Given the triple- $\mathbf{q}$  CDW nature of  $2H$  group V TMDs [46], these results suggest a commensurate  $3 \times 3$  CDW structure in the latter two monolayers [47,48] but an incommensurate CDW structure close to a  $3 \times 3$  ordering in the former one [49,50], which had been well verified by scanning tunneling microscopy (STM) [15,16,19,51–53]. For  $1H-NbS_2$ , the lowest-energy phonon mode is localized at  $0.74\Gamma M$ , also pointing to incommensurate distortions with a periodicity not far from  $3 \times 3$ , in line with the CDW observed for  $1H-NbS_2$  on  $6H-SiC(0001)$  [18]. Notice that despite the removal of charge ordering in bulk  $2H-NbS_2$  due to anharmonicity [54,55], in monolayer  $1H-NbS_2$  the CDW could survive as a result of enhanced tendency toward CDW in the 2D limit, as demonstrated by recent anharmonic phonon calculations [55].

Bulk  $2H-TX_2$  has been known to show CDWs driven by strong EPC, instead of a purely electronic CDW due to the lack of required divergence in the real part of electronic susceptibility [22,25]. It is still unclear whether this picture holds in  $1H-TX_2$  monolayer, as reduced dimensionality may strengthen electronic instabilities associated with Fermi-surface nesting. To get insight into the origin of CDWs

in  $1H\text{-}TX_2$ , I calculate the phonon linewidth of the soft LA branch,

$$\gamma_{\mathbf{q}} = \frac{2\pi\omega_{\mathbf{q}}}{N_{\mathbf{k}}} \sum_{\mathbf{k}} |g_{\mathbf{k},\mathbf{k}+\mathbf{q}}|^2 \delta(\epsilon_{\mathbf{k}} - \epsilon_F) \delta(\epsilon_{\mathbf{k}+\mathbf{q}} - \epsilon_F), \quad (1)$$

and both the real and imaginary parts of bare susceptibility in the constant matrix element approximation [25],

$$\chi_0'(\mathbf{q}) = \sum_{\mathbf{k}} \frac{f(\epsilon_{\mathbf{k}+\mathbf{q}}) - f(\epsilon_{\mathbf{k}})}{\epsilon_{\mathbf{k}} - \epsilon_{\mathbf{k}+\mathbf{q}}}, \quad (2)$$

$$\lim_{\omega \rightarrow 0} \chi_0''(\mathbf{q}, \omega)/\omega = \sum_{\mathbf{k}} \delta(\epsilon_{\mathbf{k}} - \epsilon_F) \delta(\epsilon_{\mathbf{k}+\mathbf{q}} - \epsilon_F), \quad (3)$$

along the high-symmetry directions  $\Gamma\text{-}M\text{-}K\text{-}\Gamma$ , as plotted in Figs. 1(e) and 1(f). For all  $1H\text{-}TX_2$  with similar half-filled  $d$  bands at  $E_F$  [Fig. 1(c)], the maximum of Fermi-surface nesting [ $\zeta(\mathbf{q}) = \lim_{\omega \rightarrow 0} \chi_0''(\mathbf{q}, \omega)/\omega$ ] locates near the  $K$  point [Fig. 1(f)], reflecting partial nesting between the hexagonal  $\Gamma$  and triangular  $K$  pockets. However, no nesting-driven peak is found in  $\zeta(\mathbf{q})$  at  $\mathbf{q}_{\text{CDW}}$ , and only a broad maximum at  $\mathbf{q}_{\text{CDW}}$  appears in  $\chi_0'(\mathbf{q})$ , which is somewhat too weak to trigger a CDW transition. On the other hand, the linewidth of the LA branch displays a sharp peak around  $\mathbf{q}_{\text{CDW}}$  [Fig. 1(e)] indicating strong momentum dependence of the electron-phonon matrix elements  $g_{\mathbf{k},\mathbf{k}+\mathbf{q}}$ , which coincides with its phonon instability area shown in Fig. 1(a). Obviously, it is not the Fermi-surface nesting, but the  $\mathbf{q}$ -dependent EPC that is responsible for CDWs in  $1H\text{-}TX_2$  monolayers.

## B. Modulated lattice and relative CDW strength

In comparison with an electronic CDW where long-range order and incommensurability emerge with lattice distortion as only a by-product caused by a finite EPC, a strong-coupling CDW possesses a larger distortion amplitude signifying strong EPC, a larger energy gap, and a shorter coherence length [46]. With much more distinct atomic displacements, the atoms tend to form clusters with shortened bonds and the CDW modulation tends to be commensurate via locking into the underlying lattice. Below I conduct a fully commensurate analysis for the  $3 \times 3$  CDW order in monolayer  $1H\text{-}TX_2$  to study their structural atomic rearrangements and superconducting properties. Such a treatment has been suggested to well explain the modulated lattice, Raman CDW modes as well as the coexistence of competing modulations for  $1H\text{-}NbSe_2$  in spite of its CDW's slight incommensurability [49,52].

Full optimization of  $3 \times 3$  superstructures of  $1H\text{-}TX_2$  with the soft-mode derived atomic distortion or randomized ones results in a common equilibrium CDW phase for all studied monolayers, shown in Fig. 2(a). This distorted structure contains triangular three- and six-atom  $T$  clusters centered on the honeycomb-lattice hollow sites. Out of three inequivalent  $T$  atoms, the atoms in the  $T$  trimer (denoted by 1) exhibit the largest in-plane displacement toward a hollow site, thus generating the shortest Nb-Nb or Ta-Ta bonds. Notice that for monolayer  $NbSe_2$ ,  $TaSe_2$ , and  $NbS_2$ , the inclusion of SOC does not change the pattern of the CDW modulation, while for monolayer  $TaS_2$ , it induces further atomic rearrangement leading to another distorted structure

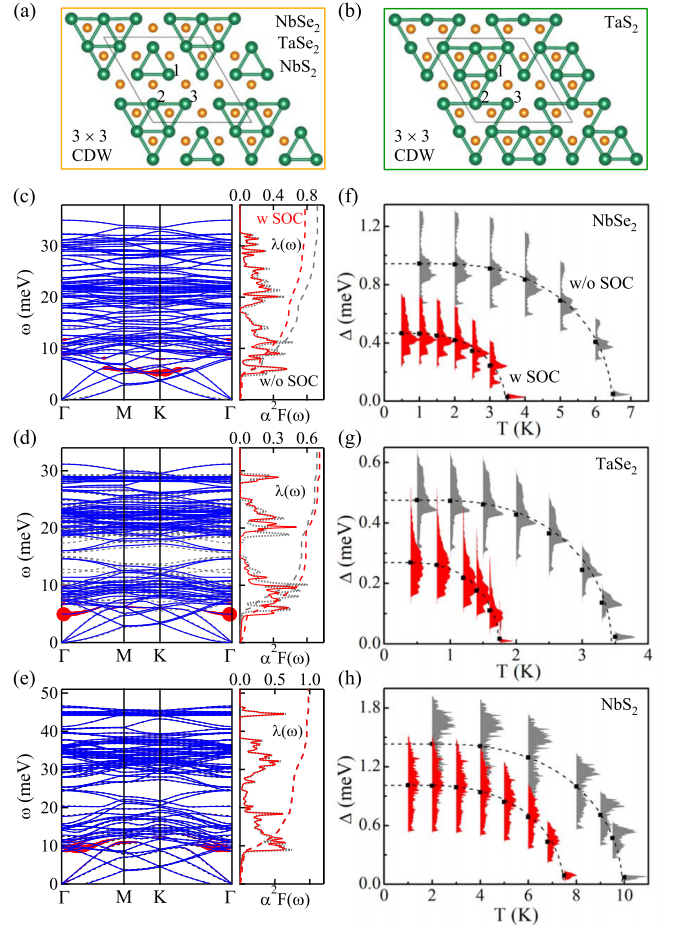


FIG. 2. (a), (b) Crystal structures of the ground-state  $3 \times 3$  CDW phases of monolayer  $NbSe_2$ ,  $TaSe_2$ ,  $NbS_2$  (a), and  $TaS_2$  (b) under SOC. (c)–(e) Phonon spectrum weighted by the mode EPC strength  $\lambda_{\mathbf{q}\nu}$  (red dots), isotropic Eliashberg spectral function  $\alpha^2F(\omega)$ , and frequency-dependent EPC  $\lambda(\omega)$  in the CDW state of monolayer  $NbSe_2$  (c),  $TaSe_2$  (d), and  $NbS_2$  (e). The blue solid and gray dashed lines represent the phonon results obtained with and without SOC, respectively. (f)–(h) Anisotropic superconducting gaps of monolayer  $TX_2$ 's CDW phase on the Fermi surface as a function of temperature, calculated with (red) and without SOC (gray) using the anisotropic Migdal-Eliashberg theory. The black squares indicate the average value of the gaps. The dashed lines are fits obtained by solving numerically the BCS gap equation using the average  $\Delta_0$  and  $T_c$  from first-principles calculations.

depicted in Fig. 2(b), which shows a continuous pattern of overlapping triangular six-atom Ta clusters of two different types with or without shortened Ta-Ta bonds inside the large triangles [47]. It needs to be emphasized that the above two CDW structures display a unique hollow-centered distortion of transition-metal atoms; this kind of clustering favors  $T\text{-}T$  interactions and has advantage in lowering the energy of the system over other atom-centered ones (e.g., the  $T$ -centered hexagonal/star-shaped clustering [52,56] or  $X$ -centered triangular clustering [47–49]), therefore constituting the ground-state CDW phase for each  $1H\text{-}TX_2$  monolayer. Remarkably, STM simulations [48,49] for the hollow-centered structure in Fig. 2(a) had successfully reproduced the

TABLE I. The lattice constant  $a$  of monolayer  $1H-TX_2$ , the maximum transition-metal atomic displacement  $\delta T$  of its  $3 \times 3$  CDW phase, the ratio  $\delta T/a$ , the Fermi-level DOS  $N_F^{\text{nor}}$  and  $N_F^{\text{CDW}}$  in the normal and CDW states, and the ratio  $\frac{N_F^{\text{CDW}}}{N_F^{\text{nor}}}$  obtained under SOC.

System	$a$ (Å)	$\delta T$ (Å)	$\delta T/a$	$N_F^{\text{nor}}$	$N_F^{\text{CDW}}$	$\frac{N_F^{\text{CDW}}}{N_F^{\text{nor}}}$
				(states/eV f.u.)		
NbSe <sub>2</sub>	3.474	0.085	2.4%	2.82	1.48	0.53
TaS <sub>2</sub>	3.34	0.061	1.8%	2.62	1.41	0.54
TaSe <sub>2</sub>	3.471	0.092	2.7%	2.66	1.23	0.46
NbS <sub>2</sub>	3.348	0.059	1.8%	2.75	2.02	0.73

experimentally observed STM images in the CDW state reported for  $1H\text{-NbSe}_2$  by Ugeda *et al.* [15] and for  $1H\text{-TaSe}_2$  by Ryu *et al.* [16].

On the basis of the determinate low-energy monolayer CDW structures, I discuss the strength of CDW order in  $1H\text{-TX}_2$  by analyzing the maximum transition-metal atomic displacement  $\delta T$  and the variation of the Fermi-level DOS  $N_F$  with respect to the normal state. The relevant data under SOC are listed in Table I. For the two diselenides  $1H\text{-NbSe}_2$  and  $1H\text{-TaSe}_2$ ,  $\delta T$  is calculated to be around 0.09 Å, evidently larger than 0.06 Å obtained for the two disulfides  $1H\text{-NbS}_2$  and  $1H\text{-TaS}_2$ . I also compare the ratio  $\delta T/a$  so as to eliminate the influence of different lattice constants  $a$  for  $1H\text{-TX}_2$ , and find a consistent trend indicating larger distortion amplitude in the diselenides than in the disulfides. In the meantime,  $N_F$  for  $1H\text{-NbSe}_2$ ,  $1H\text{-TaS}_2$ , and  $1H\text{-TaSe}_2$  is found to be largely reduced from 2.6–2.8 states/eV f.u. in the normal state to 1.2–1.5 states/eV f.u. in the CDW state, yielding a ratio  $\frac{N_F^{\text{CDW}}}{N_F^{\text{nor}}}$  around 0.5 which implies a significant CDW-induced energy gapping in these three monolayers. However, only a moderate reduction of  $N_F$  is seen for  $1H\text{-NbS}_2$ , although it has nearly the same CDW distortion amplitude as  $1H\text{-TaS}_2$ . Combining the  $\delta T$  and  $N_F$  results, I can conclude that the CDW order is strongest in  $1H\text{-NbSe}_2$  and  $1H\text{-TaSe}_2$ , intermediate in  $1H\text{-TaS}_2$ , and weakest in  $1H\text{-NbS}_2$ . This relative CDW strength is supported by recent Raman studies of CDW transition temperatures in exfoliated  $1H\text{-TX}_2$  monolayers [13,14], noticing that disorder from sample degradation would be detrimental to CDW and affect accuracy of the measured transition temperature. In addition, the aforementioned CDW-modulated electronic features could not only help understand the different superconducting  $T_c$  of  $1H\text{-TX}_2$  (Table II), but also offer key clues for clarifying their  $T_c$  variation trend compared to the bulk case.

### C. Monolayer superconductivity

I now turn to investigate the superconducting properties of  $1H\text{-TX}_2$  in the CDW state, a comprehensive understanding of which was theoretically limited. Moreover, it is also interesting to explore the importance of SOC in determining the superconductivity by examining its modification effects on electron-phonon properties and critical temperature  $T_c$ , which were usually neglected in previous calculations on superconducting group V TMDs [11,48,49,54,57–60]. With the

TABLE II. The isotropic EPC strength  $\lambda$ , critical temperature  $T_c$  derived from anisotropic Migdal-Eliashberg equations, and superconducting gap  $\Delta_0$  in the  $T = 0$  K limit for monolayer  $1H\text{-TX}_2$  in  $3 \times 3$  CDW state, compared to available experimental data.

System	w/o SOC			w SOC			Expt. $T_c$ (K)
	$\lambda$	$T_c$ (K)	$\Delta_0$ (meV)	$\lambda$	$T_c$ (K)	$\Delta_0$ (meV)	
NbSe <sub>2</sub>	0.92	6.5	0.94	0.77	3.5	0.46	3.1 – 3.5 <sup>a</sup>
TaS <sub>2</sub>	1.15	13	1.95	0.79	3.1	0.47	3 – 3.4 <sup>b</sup>
TaSe <sub>2</sub>	0.69	3.5	0.48	0.71	1.8	0.27	1 – 1.4 <sup>c</sup>
NbS <sub>2</sub>	0.98	10	1.43	0.98	7.5	1.01	2 – 3 <sup>d</sup>

<sup>a</sup> $1H$  [26,27].

<sup>b</sup> $1H$  [17,30].

<sup>c</sup>Multilayer [31,32].

<sup>d</sup>Multilayer [33,34].

identified low-energy distorted structures, I calculate CDW state's phonon spectrum for monolayer NbSe<sub>2</sub>, TaSe<sub>2</sub>, and NbS<sub>2</sub> without and with SOC, as plotted in left panels of Figs. 2(c)–2(e) where the size of red dots is proportional to the EPC strength of each phonon mode,  $\lambda_{\mathbf{qv}} = \gamma_{\mathbf{qv}}/(\pi N_F \omega_{\mathbf{qv}}^2)$ , in case of SOC. The isotropic Eliashberg spectral function obtained from electron-phonon Wannier interpolation [43],

$$\alpha^2 F(\omega) = \frac{1}{2N_{\mathbf{q}}} \sum_{\mathbf{qv}} \lambda_{\mathbf{qv}} \omega_{\mathbf{qv}} \delta(\omega - \omega_{\mathbf{qv}}), \quad (4)$$

and the frequency-dependent EPC,

$$\lambda(\omega) = 2 \int_0^\omega \frac{\alpha^2 F(\omega')}{\omega'} d\omega', \quad (5)$$

are shown in right panels of Figs. 2(c)–2(e) (see data for  $1H\text{-TaS}_2$  in Ref. [47]). Clearly, for all  $1H\text{-TX}_2$ , dynamical stability of the CDW phase is confirmed, and it is the low-energy modes originating from mainly the vibrations of heavier  $T$  atoms that dominate the coupling with  $d$  electrons around  $E_F$ , as evidenced by the large Eliashberg function  $\alpha^2 F(\omega)$  and rapid increase of the integrated EPC  $\lambda(\omega)$  in the corresponding low-energy region.

As found from Figs. 2(c)–2(e), upon the inclusion of SOC, the total EPC  $\lambda = 2 \int_0^\infty \alpha^2 F(\omega)/\omega d\omega$  is reduced from 0.92 to 0.77 for  $1H\text{-NbSe}_2$  (similar to  $1H\text{-TaS}_2$  whose  $\lambda$  decreases from 1.15 to 0.79 [47]), while it slightly increases from 0.69 to 0.71 for  $1H\text{-TaSe}_2$  and remains unchanged (0.98) for  $1H\text{-NbS}_2$ . The varied behaviors of  $\lambda$  in these systems are directly related to the evolution of the peak intensity and position of  $\alpha^2 F(\omega)$  under SOC, which could reflect the delicate influence SOC exerts on the electron-phonon matrix elements and phonon frequencies of each system. For both  $1H\text{-NbSe}_2$  [Fig. 2(c)] and  $1H\text{-TaS}_2$ , the mode EPC strength  $\lambda_{\mathbf{qv}}$  ( $\nu = 1\text{--}27$ , folded from  $1 \times 1$  phase's three acoustic modes) of the CDW phase is reduced in most of the Brillouin zone after including the SOC, resulting in the decline of peak intensity in low-energy part of  $\alpha^2 F(\omega)$  with its peak position changing little. Since SOC has relatively weak effect on the CDW electronic structure, the weakening of the EPC strength in CDW state is not expected to arise from the Fermi-surface change, but mainly due to the SOC-induced suppression of

the matrix elements  $g_{\mathbf{k},\mathbf{k}+\mathbf{q}}^{\nu}$  of those low-energy  $T$ -dominated phonon modes [47]. Furthermore, owing to the larger atomic SOC contribution from Ta atoms than that from Nb atoms, this suppression effect is more significant in  $1H$ -TaS<sub>2</sub> than in  $1H$ -NbSe<sub>2</sub>, leading to greater decrease of total  $\lambda$  in the former. In comparison with  $1H$ -TaS<sub>2</sub>, the reduction of  $\lambda_{q\nu}$  ( $\nu = 1-27$ ) is weaker in  $1H$ -TaSe<sub>2</sub> because of an obvious softening of low-energy phonon modes under SOC [Fig. 2(d)], despite a similar suppression of their electron-phonon matrix elements. The peak intensity of  $\alpha^2F(\omega)$  in low-energy region thus only slightly declines; however, its peak position shows a considerable redshift due to the decreased phonon frequencies, eventually leading to a minor increase of total  $\lambda$  in  $1H$ -TaSe<sub>2</sub>, according to Eq. (5). Additionally, both the peak intensity and position of  $\alpha^2F(\omega)$  for  $1H$ -NbS<sub>2</sub> are nearly unaffected by SOC [Fig. 2(e)] implying little influence on its phonon spectrum and EPC strength.

To evaluate the critical temperature  $T_c$  and get insight into the nature of the superconducting gap, I employ the fully anisotropic Migdal-Eliashberg theory [44,45] to study the superconductivity in  $1H$ - $TX_2$  monolayers, instead of using the ordinary Allen-Dynes modified McMillan equation [61] which relies strongly on the isotropic EPC parameter  $\lambda$  in estimating  $T_c$ . Figures 2(f)–2(h) show the energy distribution of temperature-dependent superconducting gaps  $\Delta_{\mathbf{k}}$  on the Fermi surface for monolayer  $TX_2$ 's CDW phase (see data for  $1H$ -TaS<sub>2</sub> in Ref. [47]), calculated without and with SOC by solving the anisotropic Eliashberg equations at an effective Coulomb pseudopotential  $\mu^*$  that is chosen according to prior studies on  $2H$  group V TMDs [11,48,54]. Overall, regardless of SOC, the monolayers studied all exhibit a single anisotropic full-gap superconducting order, being relevant to the CDW-caused significant reduction of in-plane  $Td$  states around  $E_F$  that are crucial for forming a separated larger gap. For  $1H$ -NbSe<sub>2</sub> [Fig. 2(f)] and  $1H$ -TaS<sub>2</sub>, the superconducting gap in the absence of SOC diminishes gradually with increasing temperature and is seen to vanish at  $T_c = 6.5$  and 13 K, respectively, both of which seriously deviate from the experimentally observed critical temperatures of 3.1–3.5 [26,27] and 3–3.4 K [17,30] in these two monolayers. By contrast, once SOC is introduced into superconducting calculations, their corresponding  $T_c$  are found to respectively decrease to 3.5 and 3.1 K, matching well with experiments. Such a marked modification of  $T_c$  results mainly from the SOC-induced weakening of total EPC  $\lambda$ . On the other hand, for  $1H$ -TaSe<sub>2</sub> and  $1H$ -NbS<sub>2</sub> [Figs. 2(g) and 2(h)], though the total  $\lambda$  almost unchanged, the inclusion of SOC still causes a considerable decrease of their predicted  $T_c$  to 1.8 and 7.5 K (see their averaged gap  $\Delta_0$  in the  $T = 0$  K limit in Table II). These findings suggest that the magnitude of  $T_c$  in a TMD not only correlates with its isotropic EPC strength, but also depends on the anisotropic treatment of its electron-phonon and superconducting properties, where the extent of EPC anisotropy and thus the critical temperature can be affected by SOC.

As a matter of fact, in layered or 2D systems with multi-sheet Fermi surfaces, anisotropic electron-phonon interactions are very essential for correctly describing the superconductivity, whereas predicting  $T_c$  within only the isotropic approximation may be insufficient in most cases. In order to quantify the EPC anisotropy in monolayer  $TX_2$ 's CDW phase,

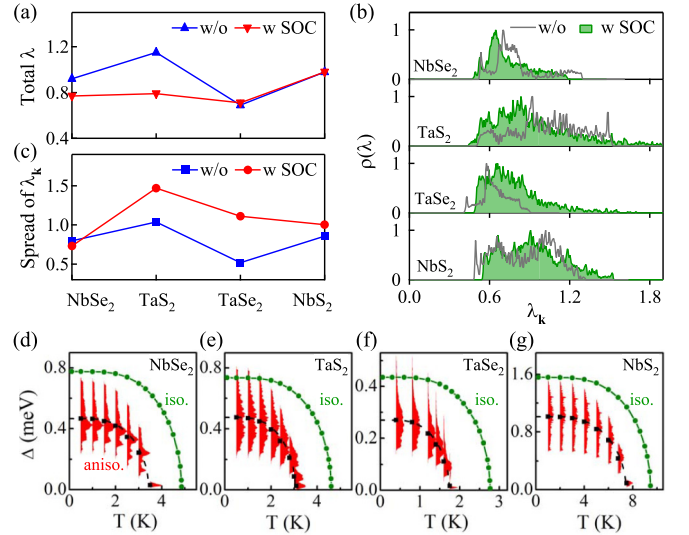


FIG. 3. (a)–(c) Comparison of the total coupling strength  $\lambda$  (a), the distribution of the EPC strength  $\lambda_{\mathbf{k}}$  of each electronic state around  $E_F$  (b), and the spread of  $\lambda_{\mathbf{k}}$  reflecting the extent of EPC anisotropy (c) between the two cases with and without SOC for monolayer  $1H$ - $TX_2$  in  $3 \times 3$  CDW state. (d)–(g) Comparison of the temperature-dependent superconducting gaps obtained from the isotropic Migdal-Eliashberg theory under SOC (green circles) with the corresponding anisotropic gap data for monolayer  $TX_2$ 's CDW phase.

I evaluate the momentum-resolved EPC strength on the Fermi surface, defined as [44]

$$\lambda_{\mathbf{k}} = \sum_{\mathbf{k}',\nu} \delta(\epsilon_{\mathbf{k}'} - \epsilon_F) |g_{\mathbf{k}\mathbf{k}'}^{\nu}|^2 / \omega_{\mathbf{k}-\mathbf{k}'\nu}. \quad (6)$$

Figures 3(b) and 3(c) plot the distribution of  $\lambda_{\mathbf{k}}$  of each electronic state around  $E_F$  and the spread of  $\lambda_{\mathbf{k}}$ , respectively. Obviously, compared with the case without SOC,  $\lambda_{\mathbf{k}}$  under SOC in general shows a broader distribution as a consequence of the SOC-derived energy splitting of  $d$  bands in proximity of the Fermi surface, indicating stronger EPC anisotropy. In particular, for  $1H$ -TaS<sub>2</sub> and  $1H$ -TaSe<sub>2</sub>, the spread of  $\lambda_{\mathbf{k}}$  exhibits the largest expansion due to the rather significant SOC strength and spin-orbit splitting in Ta-based TMDs [see Fig. 1(d)]. What matters most is that, for all studied monolayers, the renormalized  $\lambda_{\mathbf{k}}$  by SOC tends to be concentrated in the lower side of its distribution, implying the majority of electronic states are involved in relatively weak electron-phonon scattering processes and pairing potentials for them thus are more easily destroyed by increasing the temperature. The above analysis in terms of the anisotropic EPC strength could, on top of the variation of an isotropic  $\lambda$  parameter [Fig. 3(a)], explain the concurrent decrease of the superconducting  $T_c$  of monolayer  $1H$ - $TX_2$  upon inclusion of the SOC effects.

Combining Figs. 3(c) and 3(a), I find in  $1H$ -NbSe<sub>2</sub> a slight contraction of the spread of  $\lambda_{\mathbf{k}}$  (probably associated with a particularly large Fermi-surface energy gapping due to CDW), and it seems like that an isotropic treatment of the EPC would be proper for evaluating the  $T_c$ . This argument is, however, untenable since addressing the detailed anisotropic

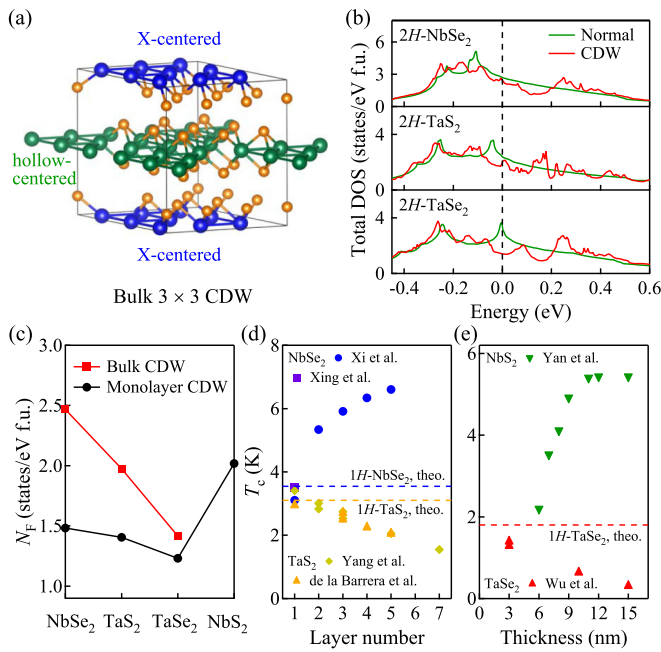


FIG. 4. (a) Crystal structure of bulk  $2H-TX_2$ 's  $3 \times 3$  CDW phase, formed by alternating stacking of two monolayer CDW structures with hollow- (green) and X-centered (blue) triangular  $T$  clusters. (b) Total electronic DOS for the bulk normal and CDW phases under SOC. The Fermi-surface average for SOC-induced energy splitting of normal phase's two  $d$  bands,  $\Delta_{SO}$  is 0.012 eV for  $2H-NbS_2$ , 0.032 eV for  $2H-NbSe_2$ , 0.113 eV for  $2H-TaS_2$ , and 0.12 eV for  $2H-TaSe_2$  [62], smaller than those in corresponding monolayers [Fig. 1(d)]. (c) Comparison of the Fermi-level DOS  $N_F$  in the bulk and monolayer CDW states. (d), (e) Experimental superconducting  $T_c$  of  $2H-TX_2$  as a function of layer number ( $NbSe_2$  [26,27],  $TaS_2$  [17,30]) (d) or thickness ( $TaSe_2$  [32],  $NbS_2$  [33]) (e), along with the theoretical  $T_c$  of monolayer  $1H-TX_2$  (horizontal dashed lines).

EPC takes into account the real Fermi surface of a TMD and has advantage over the isotropic treatment in interpreting the experimental data, as confirmed by my additional calculations based on the isotropic Eliashberg equations under SOC, where the resulting  $T_c$  is consistently higher than that derived from the corresponding anisotropic calculations [Figs. 3(d)–3(g)]. This further demonstrates the indispensable role anisotropic electron-phonon interactions play in low-dimensional superconducting systems.

#### D. CDW and superconductivity in bulk $2H-TX_2$

Current research interest in layered  $2H$  group V TMDs is partly aroused by the mechanisms behind the complicated behaviors of their superconducting  $T_c$  as a function of thickness. For  $2H-NbSe_2$ ,  $T_c$  decreases gradually with decreasing layer number [26,27], whereas in  $2H-TaS_2$  the opposite trend is observed with its  $T_c$  consecutively rising down to the monolayer limit [17,30] [Fig. 4(d)]. Also, an increasing (decreasing) trend of  $T_c$  relative to the bulk is found in multilayer  $2H-TaSe_2$  ( $2H-NbS_2$ ) [Fig. 4(e)], although data in the corresponding monolayers were so far not reported due to severe sample degradation [31–34]. To uncover the physical origins underlying such varied superconducting trends, it is necessary to

clarify the thickness dependencies of the coexisting CDW order as well as the electron-phonon interactions.

In principle, elucidating the evolution of CDW from bulk to monolayer  $TX_2$  is the first important step, as the CDW-induced energy gapping around  $E_F$  modifies the Fermi-level DOS  $N_F$  and thus the number of charge carriers available for Cooper pairing, which will largely determine the total EPC  $\lambda$  and superconducting  $T_c$  in the CDW state. Below I perform a careful analysis of the CDW structural and electronic properties of bulk  $2H-TX_2$  and make comparisons with their monolayer counterparts. Full optimization of the  $3 \times 3$  superstructures with different initial atomic distortions yields a common low-energy bulk CDW phase for  $2H-NbSe_2$ ,  $2H-TaS_2$ , and  $2H-TaSe_2$  [see Fig. 4(a)], which is featured by alternating stacking of two monolayer CDW structures that contain triangular three- and six-atom  $T$  clusters centered on the lattice hollow sites and the  $X$  atoms, respectively [49]. For these three systems, I calculate their bulk electronic DOS under SOC in both the normal and CDW phases, as shown in Fig. 4(b). The Fermi-surface energy gapping by CDW is seen to get strengthened with the  $N_F$  in CDW state rapidly reduced [Fig. 4(c)] when going from bulk  $NbSe_2$  to  $TaS_2$  ( $TaSe_2$ ), which coincides with the trends in their measured CDW and superconducting transition temperatures [5–8], i.e., the former increases from 33 K to 75 (120) K while the latter decreases from 7 K to 0.8 (0.1) K. This provides strong support for the bulk CDW structural model identified here and the key impact  $N_F$  has on the bulk EPC and superconductivity (despite the distinct phonon spectra and matrix elements).

I then compare in Fig. 4(c) the resulting Fermi-level DOS for bulk  $2H-TX_2$ 's CDW phase with that obtained earlier for the monolayer CDW phase. It is found that the value of  $N_F$  in the CDW state is in general lower in the monolayer as compared to the bulk; given the very close  $N_F$  in the bulk and monolayer normal states, this indicates a stronger electronic DOS modulation and therefore an enhanced CDW order in the 2D limit of  $2H-TX_2$ . In particular, the intensified CDW-induced modulation of  $N_F$  from bulk to monolayer is much more significant in  $NbSe_2$  than in  $TaS_2$  and  $TaSe_2$ . Such a prominent enhancement of CDW in  $NbSe_2$  has been well established in Raman experiments on its atomically thin films showing a sharply rising CDW transition temperature with decreasing thickness [13,14]. Considering that CDW ordering could also emerge in the monolayer thickness of  $2H-NbS_2$  which shows no CDW in the bulk [18], I emphasize that the tendency of enhanced CDW in monolayer limit suggested by current theoretical calculations would be universal in metallic TMDs in light of the EPC nature of their CDW formation and the strengthened electron-phonon interactions under reduced dimensionality (reflected by the increased LA branch's phonon linewidth from bulk to monolayer).

It is noteworthy that the situation concerning the evolution of CDW in 2D Ta-based TMDs is currently still unclear from experiments: whereas angle-resolved photoelectron spectroscopy studies found a slightly strengthened CDW in the epitaxial  $TaSe_2$  monolayer [16], no CDW was revealed in transport studies of the encapsulated  $TaS_2$  monolayer [17]; besides, the very recent Raman studies on exfoliated  $TaS_2$  and  $TaSe_2$  monolayers reported CDW transition temperatures comparable with those in the corresponding bulk cases [14]. I

attribute these discrepancies to the differences in sample quality or environment, and unambiguous evidence for a stronger CDW in 2D TaS<sub>2</sub> and TaSe<sub>2</sub> is yet to be clarified.

### E. Origins of distinct thickness-dependent trends of $T_c$ in NbX<sub>2</sub> and TaX<sub>2</sub>

With the basic knowledge of changes of the  $N_F$  under CDW modulation and the associated electron-phonon physics upon thickness reduction, I now discuss two different scenarios for the varied thickness dependencies of superconductivity in  $2H-TX_2$ . For  $2H-NbSe_2$ , as the layer number decreases, the Fermi-surface gapping in the CDW phase strengthens greatly as a result of the rapidly enhanced CDW, leading to a largely reduced Fermi-level DOS. The substantial diminishment of electronic states available for Cooper pairing in 2D limit is expected to dominate over the changes in phonon spectra (softened due to less interlayer restriction) and electron-phonon matrix elements (reinforced due to weaker dielectric screening), giving rise to significant weakening of total EPC strength and thus superconductivity with decreasing thickness. Hence, a strong competitive interaction between CDW and superconductivity [49] is responsible for the continued suppression of experimentally observed  $T_c$  in atomically thin NbSe<sub>2</sub>.

On the other hand, as the layer number is reduced for  $2H-TaS_2$  and  $2H-TaSe_2$ , the Fermi-level DOS of the CDW phase slowly diminishes with respect to the bulk owing to the strengthened CDW, yielding only a moderate or slight decrease in the number of electrons for pairing in monolayer limit of the two systems. This leaves room for other factors such as the variations of phonon spectra and matrix elements to determine the trends of  $\lambda$  and  $T_c$  under reduced dimensionality. Based on  $\lambda \sim \frac{N_F \langle g^2 \rangle}{M \langle \omega^2 \rangle}$  [63], smaller  $\langle \omega^2 \rangle$  (the average of the square of phonon frequency) and larger  $\langle g^2 \rangle$  (the average over the Fermi surface of the square of electron-phonon matrix element) can increase  $\lambda$  in the monolayer limit given a relatively weak change in  $N_F$ . Actually, accompanied with the enhancement of CDW, the phonon linewidth for almost the entire LA branch of the normal phase (not just at  $\mathbf{q}_{CDW}$ ) rises markedly from bulk to monolayer TaS<sub>2</sub> or TaSe<sub>2</sub>, reflecting strongly strengthened electron-phonon matrix elements [47,48]. Furthermore, since this soft LA branch has much greater matrix elements than normal phase's other two acoustic branches, the dimensionality-induced rise of its original EPC in normal state will synchronously affect the total EPC in CDW state dominated by the low-energy CDW folded acousticlike modes (see Fig. 2). This synergistic behavior, lying in a close relation between the EPCs dictating the CDW and superconductivity, suggests a cooperative interaction

between the two collective orders [47] that is responsible for the increase of  $T_c$  as TaS<sub>2</sub> or TaSe<sub>2</sub> is thinned to 2D limit.

Finally, I comment that whether a declining (rising)  $\lambda$  occurs in 2D NbSe<sub>2</sub> (TaS<sub>2</sub> and TaSe<sub>2</sub>) remains to be confirmed via direct phonon and electron-phonon calculations for bulk  $2H-TX_2$ 's CDW phase under SOC, which require huge computational resources beyond my limited capacity. In case of  $2H-NbS_2$  with no bulk CDW order, a prior theoretical work found  $\lambda = 1.5$  and a Migdal-Eliashberg  $T_c$  of 18.6 K in the bulk [54], larger than  $\lambda = 0.98$  and  $T_c$  of 7.5 K calculated for its monolayer CDW phase. Here the decline of the monolayer predicted  $\lambda$  and  $T_c$  is consistent with the suppressed  $T_c$  observed in atomically thin NbS<sub>2</sub>, in spite of an overestimation by theory of the measured  $T_c$  for this system. I therefore expect in the 2D limit of NbS<sub>2</sub> a similar exclusive interaction of CDW and superconductivity as in the NbSe<sub>2</sub> case.

## IV. CONCLUSIONS

I theoretically explore the CDW formation mechanism, low-energy CDW phase, and superconductivity in monolayer  $1H-TX_2$  with  $T = Nb, Ta$  and  $X = S, Se$  as well as the dimensionality effects on collective orders in these group V TMDs. Phonon and susceptibility results demonstrate the strongly momentum-dependent EPC, rather than Fermi-surface nesting, as the origin of CDW instability. A  $3 \times 3$  distorted structure displaying hollow-centered clustering of transition-metal atoms constitutes the ground-state CDW phase for each monolayer. Electron-phonon and Migdal-Eliashberg theory results reveal that SOC effects renormalize the superconducting critical temperature  $T_c$  in CDW state by modifying both its isotropic coupling strength  $\lambda$  and the extent of EPC anisotropy. From bulk to monolayer the intensified Fermi-surface gapping by CDW points to a generally enhanced CDW order, and depending on the  $N_F$  variation, either competitive or cooperative interaction of CDW with superconductivity can be anticipated through the delicate balance between CDW-induced diminishment of electronic states available for pairing and strengthened electron-phonon matrix elements in the reduced dimensionality. The two physical scenarios should lie behind the complex behaviors of  $T_c$  observed down to monolayer limit of  $2H$  group V TMDs, and also serve as basic mechanisms for explaining superconductivity in other atomically thin CDW metals.

## ACKNOWLEDGMENTS

I gratefully thank Christoph Heil and Wenhui Duan for helpful discussions. This work is supported by the National Natural Science Foundation of China (Grant No. 11904325) and the National Supercomputing Center in Zhengzhou.

- [1] C.-W. Chen, J. Choe, and E. Morosan, Charge density waves in strongly correlated-electron systems, *Rep. Prog. Phys.* **79**, 084505 (2016).  
 [2] H. Yang, S. W. Kim, M. Chhowalla, and Y. H. Lee, Structural and quantum-state phase transitions in van der Waals layered materials, *Nat. Phys.* **13**, 931 (2017).

- [3] J. A. Wilson, F. J. Di Salvo, and S. Mahajan, Charge-density waves and superlattices in the metallic layered transition metal dichalcogenides, *Adv. Phys.* **50**, 1171 (2001).  
 [4] A. H. Castro Neto, Charge Density Wave, Superconductivity, and Anomalous Metallic Behavior in 2D Transition Metal

- Dichalcogenides Superconductivity, *Phys. Rev. Lett.* **86**, 4382 (2001).
- [5] D. E. Moncton, J. D. Axe, and F. J. Di Salvo, Study of Superlattice Formation in  $2H$ -NbSe<sub>2</sub> and  $2H$ -TaSe<sub>2</sub> by Neutron Scattering, *Phys. Rev. Lett.* **34**, 734 (1975).
- [6] Z. Dai, Q. Xue, Y. Gong, C. G. Slough, and R. V. Coleman, Scanning-probe-microscopy studies of superlattice structures and density-wave structures in  $2H$ -NbSe<sub>2</sub>,  $2H$ -TaSe<sub>2</sub>, and  $2H$ -TaS<sub>2</sub> induced by Fe doping, *Phys. Rev. B* **48**, 14543 (1993).
- [7] Y. Kvashnin, D. VanGennep, M. Mito, S. A. Medvedev, R. Thiyagarajan, O. Karis, A. N. Vasiliev, O. Eriksson, and M. Abdel-Hafiez, Coexistence of Superconductivity and Charge Density Waves in Tantalum Disulfide: Experiment and Theory, *Phys. Rev. Lett.* **125**, 186401 (2020).
- [8] T. Yokoya, T. Kiss, A. Chainani, S. Shin, M. Nohara, and H. Takagi, Fermi surface sheet-dependent superconductivity in  $2H$ -NbSe<sub>2</sub>, *Science* **294**, 2518 (2001).
- [9] I. Guillamón, H. Suderow, S. Vieira, L. Cario, P. Diener, and P. Rodière, Superconducting Density of States and Vortex Cores of  $2H$ -NbS<sub>2</sub>, *Phys. Rev. Lett.* **101**, 166407 (2008).
- [10] H. Suderow, V. G. Tissen, J. P. Brison, J. L. Martínez, and S. Vieira, Pressure Induced Effects on the Fermi Surface of Superconducting  $2H$ -NbSe<sub>2</sub>, *Phys. Rev. Lett.* **95**, 117006 (2005).
- [11] M. Leroux, I. Errea, M. Le Tacon, S. M. Souliou, G. Garbarino, L. Cario, A. Bosak, F. Mauri, M. Calandra, and P. Rodière, Strong anharmonicity induces quantum melting of charge density wave in  $2H$ -NbSe<sub>2</sub> under pressure, *Phys. Rev. B* **92**, 140303(R) (2015).
- [12] D. C. Freitas, P. Rodière, M. R. Osorio, E. Navarro-Moratalla, N. M. Nemes, V. G. Tissen, L. Cario, E. Coronado, M. García-Hernández, S. Vieira, M. Núñez-Regueiro, and H. Suderow, Strong enhancement of superconductivity at high pressures within the charge-density-wave states of  $2H$ -TaS<sub>2</sub> and  $2H$ -TaSe<sub>2</sub>, *Phys. Rev. B* **93**, 184512 (2016).
- [13] X. Xi, L. Zhao, Z. Wang, H. Berger, L. Forró, J. Shan, and K. F. Mak, Strongly enhanced charge-density-wave order in monolayer NbSe<sub>2</sub>, *Nat. Nanotechnol.* **10**, 765 (2015).
- [14] D. Lin, S. Li, J. Wen, H. Berger, L. Forró, H. Zhou, S. Jia, T. Taniguchi, K. Watanabe, X. Xi, and M. S. Bahramy, Patterns and driving forces of dimensionality-dependent charge density waves in  $2H$ -type transition metal dichalcogenides, *Nat. Commun.* **11**, 2406 (2020).
- [15] M. M. Ugeda, A. J. Bradley, Y. Zhang, S. Onishi, Y. Chen, W. Ruan, C. Ojeda-Aristizabal, H. Ryu, M. T. Edmonds, H.-Z. Tsai *et al.*, Characterization of collective ground states in single-layer NbSe<sub>2</sub>, *Nat. Phys.* **12**, 92 (2016).
- [16] H. Ryu, Y. Chen, H. Kim, H.-Z. Tsai, S. Tang, J. Jiang, F. Liou, S. Kahn, C. Jia, A. A. Omrani *et al.*, Persistent charge-density-wave order in single-layer TaSe<sub>2</sub>, *Nano Lett.* **18**, 689 (2018).
- [17] Y. Yang, S. Fang, V. Fatemi, J. Ruhman, E. Navarro-Moratalla, K. Watanabe, T. Taniguchi, E. Kaxiras, and P. Jarillo-Herrero, Enhanced superconductivity upon weakening of charge density wave transport in  $2H$ -TaS<sub>2</sub> in the two-dimensional limit, *Phys. Rev. B* **98**, 035203 (2018).
- [18] H. Lin, W. Huang, K. Zhao, C. Lian, W. Duan, X. Chen, and S.-H. Ji, Growth of atomically thick transition metal sulfide films on graphene/6H-SiC(0001) by molecular beam epitaxy, *Nano Res.* **11**, 4722 (2018).
- [19] J. Hall, N. Ehlen, J. Berges, E. van Loon, C. van Efferen, C. Murray, Malte Rösner, J. Li, B. V. Senkovskiy, M. Hell *et al.*, Environmental control of charge density wave order in monolayer  $2H$ -TaS<sub>2</sub>, *ACS Nano* **13**, 10210 (2019).
- [20] Z. Wang, Y.-Y. Sun, I. Abdelwahab, L. Cao, W. Yu, H. Ju, J. Zhu, W. Fu, L. Chu, H. Xu, and K. P. Loh, Surface-limited superconducting phase transition on  $1T$ -TaS<sub>2</sub>, *ACS Nano* **12**, 12619 (2018).
- [21] J. Shi, X. Chen, L. Zhao, Y. Gong, M. Hong, Y. Huan, Z. Zhang, P. Yang, Y. Li, Q. Zhang *et al.*, Chemical vapor deposition grown wafer-scale 2D tantalum diselenide with robust charge-density-wave order, *Adv. Mater.* **30**, 1804616 (2018).
- [22] F. Weber, S. Rosenkranz, J. P. Castellán, R. Osborn, R. Hott, R. Heid, K. P. Bohnen, T. Egami, A. H. Said, and D. Reznik, Extended Phonon Collapse and the Origin of the Charge-Density Wave in  $2H$ -NbSe<sub>2</sub>, *Phys. Rev. Lett.* **107**, 107403 (2011).
- [23] C. J. Arguello, E. P. Rosenthal, E. F. Andrade, W. Jin, P. C. Yeh, N. Zaki, S. Jia, R. J. Cava, R. M. Fernandes, A. J. Millis, T. Valla, R. M. Osgood, Jr., and A. N. Pasupathy, Quasiparticle Interference, Quasiparticle Interactions and the Origin of the Charge Density Wave in  $2H$ -NbSe<sub>2</sub>, *Phys. Rev. Lett.* **114**, 037001 (2015).
- [24] J. Diego, A. H. Said, S. K. Mahatha, R. Bianco, L. Monacelli, M. Calandra, F. Mauri, K. Rossnagel, I. Errea, and S. Blanco-Canosa, van der Waals driven anharmonic melting of the 3D charge density wave in VSe<sub>2</sub>, *Nat. Commun.* **12**, 598 (2021).
- [25] M. D. Johannes and I. I. Mazin, Fermi surface nesting and the origin of charge density waves in metals, *Phys. Rev. B* **77**, 165135 (2008).
- [26] X. Xi, Z. Wang, W. Zhao, J.-H. Park, K. T. Law, H. Berger, L. Forró, J. Shan, and K. F. Mak, Ising pairing in superconducting NbSe<sub>2</sub> atomic layers, *Nat. Phys.* **12**, 139 (2016).
- [27] Y. Xing, K. Zhao, P. Shan, F. Zheng, Y. Zhang, H. Fu, Y. Liu, M. Tian, C. Xi, H. Liu, J. Feng, X. Lin, S. Ji, X. Chen, Q.-K. Xue, and J. Wang, Ising superconductivity and quantum phase transition in macro-size monolayer NbSe<sub>2</sub>, *Nano Lett.* **17**, 6802 (2017).
- [28] X. Xi, H. Berger, L. Forró, J. Shan, and K. F. Mak, Gate Tuning of Electronic Phase Transitions in Two-Dimensional NbSe<sub>2</sub>, *Phys. Rev. Lett.* **117**, 106801 (2016).
- [29] E. Navarro-Moratalla, J. O. Island, S. Mañas-Valero, E. Pinilla-Cienfuegos, A. Castellanos-Gomez, J. Quereda, G. Rubio-Bollinger, L. Chirolli, J. A. Silva-Guillén, N. Agrait, G. A. Steele, F. Guinea, H. S. J. van der Zant, and E. Coronado, Enhanced superconductivity in atomically thin TaS<sub>2</sub>, *Nat. Commun.* **7**, 11043 (2016).
- [30] S. C. de la Barrera, M. R. Sinko, D. P. Gopalan, N. Sivadas, K. L. Seyler, K. Watanabe, T. Taniguchi, A. W. Tsen, X. Xu, D. Xiao, and B. M. Hunt, Tuning Ising superconductivity with layer and spin-orbit coupling in two-dimensional transition metal dichalcogenides, *Nat. Commun.* **9**, 1427 (2018).
- [31] J. A. Galvis, P. Rodière, I. Guillamón, M. R. Osorio, J. G. Rodrigo, L. Cario, E. Navarro-Moratalla, E. Coronado, S. Vieira, and H. Suderow, Scanning tunneling measurements of layers of superconducting  $2H$ -TaSe<sub>2</sub>: Evidence for a zero-bias anomaly in single layers, *Phys. Rev. B* **87**, 094502 (2013).
- [32] Y. Wu, J. He, J. Liu, H. Xing, Z. Mao, and Y. Liu, Dimensional reduction and ionic gating induced enhancement of superconductivity in atomically thin crystals of  $2H$ -TaSe<sub>2</sub>, *Nanotechnology* **30**, 035702 (2019).



- [33] R. Yan, G. Khalsa, B. T. Schaefer, A. Jarjour, S. Rouvimov, K. C. Nowack, H. G. Xing, and D. Jena, Thickness dependence of superconductivity in ultrathin NbS<sub>2</sub>, *Appl. Phys. Express* **12**, 023008 (2019).
- [34] Z. Wang, C.-Y. Cheon, M. Tripathi, G. M. Marega, Y. Zhao, H. G. Ji, M. Macha, A. Radenovic, and A. Kis, Superconducting 2D NbS<sub>2</sub> grown epitaxially by chemical vapor deposition, *ACS Nano* **15**, 18403 (2021).
- [35] P. Giannozzi, S. Baroni, N. Bonini, M. Calandra, R. Car, C. Cavazzoni, D. Ceresoli, G. L. Chiarotti, M. Cococcioni, I. Dabo *et al.*, QUANTUM ESPRESSO: a modular and open-source software project for quantum simulations of materials, *J. Phys.: Condens. Matter* **21**, 395502 (2009).
- [36] J. P. Perdew, K. Burke, and M. Ernzerhof, Generalized Gradient Approximation Made Simple, *Phys. Rev. Lett.* **77**, 3865 (1996).
- [37] D. R. Hamann, Optimized norm-conserving Vanderbilt pseudopotentials, *Phys. Rev. B* **88**, 085117 (2013).
- [38] M. Schlipf and F. Gygi, Optimization algorithm for the generation of ONCV pseudopotentials, *Comput. Phys. Commun* **196**, 36 (2015).
- [39] S. Grimme, J. Antony, S. Ehrlich, and H. Krieg, A consistent and accurate ab initio parametrization of density functional dispersion correction (dft-d) for the 94 elements H-Pu, *J. Chem. Phys.* **132**, 154104 (2010).
- [40] M. Methfessel and A. T. Paxton, High-precision sampling for Brillouin-zone integration in metals, *Phys. Rev. B* **40**, 3616 (1989).
- [41] S. Baroni, S. de Gironcoli, A. D. Corso, and P. Giannozzi, Phonons and related crystal properties from density-functional perturbation theory, *Rev. Mod. Phys.* **73**, 515 (2001).
- [42] G. Pizzi, V. Vitale, R. Arita, S. Bluegel, F. Freimuth, G. Géranton, M. Gibertini, D. Gresch, C. Johnson, T. Koretsune *et al.*, Wannier90 as a community code: New features and applications, *J. Phys.: Condens. Matter* **32**, 165902 (2020).
- [43] F. Giustino, M. L. Cohen, and S. G. Louie, Electron-phonon interaction using Wannier functions, *Phys. Rev. B* **76**, 165108 (2007).
- [44] E. R. Margine and F. Giustino, Anisotropic Migdal-Eliashberg theory using Wannier functions, *Phys. Rev. B* **87**, 024505 (2013).
- [45] S. Poncé, E. R. Margine, C. Verdi, and F. Giustino, EPW: Electron-phonon coupling, transport and superconducting properties using maximally localized Wannier functions, *Comput. Phys. Commun.* **209**, 116 (2016).
- [46] K. Rossnagel, On the origin of charge-density waves in select layered transition-metal dichalcogenides, *J. Phys.: Condens. Matter* **23**, 213001 (2011).
- [47] C.-S. Lian, C. Heil, X. Liu, C. Si, F. Giustino, and W. Duan, Intrinsic and doping-enhanced superconductivity in monolayer 1H-TaS<sub>2</sub>: Critical role of charge ordering and spin-orbit coupling, *Phys. Rev. B* **105**, L180505 (2022).
- [48] C.-S. Lian, C. Heil, X. Liu, C. Si, F. Giustino, and W. Duan, Coexistence of superconductivity with enhanced charge density wave order in the two-dimensional limit of TaSe<sub>2</sub>, *J. Phys. Chem. Lett.* **10**, 4076 (2019).
- [49] C.-S. Lian, C. Si, and W. Duan, Unveiling charge-density wave, superconductivity, and their competitive nature in two-dimensional NbSe<sub>2</sub>, *Nano Lett.* **18**, 2924 (2018).
- [50] F. Zheng, Z. Zhou, X. Liu, and J. Feng, First-principles study of charge and magnetic ordering in monolayer NbSe<sub>2</sub>, *Phys. Rev. B* **97**, 081101(R) (2018).
- [51] J. Dai, E. Calleja, J. Alldredge, X. Zhu, L. Li, W. Lu, Y. Sun, T. Wolf, H. Berger, and K. McElroy, Microscopic evidence for strong periodic lattice distortion in two-dimensional charge-density wave systems, *Phys. Rev. B* **89**, 165140 (2014).
- [52] B. Guster, C. Rubio-Verdú, R. Robles, J. Zaldívar, P. Dreher, M. Pruneda, J. A. Silva-Guillén, D.-J. Choi, J. I. Pascual, M. M. Ugeda, P. Ordejón, and E. Canadell, Coexistence of elastic modulations in the charge density wave state of 2H-NbSe<sub>2</sub>, *Nano Lett.* **19**, 3027 (2019).
- [53] G. Gye, E. Oh, and H. W. Yeom, Topological Landscape of Competing Charge Density Waves in 2H-NbSe<sub>2</sub>, *Phys. Rev. Lett.* **122**, 016403 (2019).
- [54] C. Heil, S. Poncé, H. Lambert, M. Schlipf, E. R. Margine, and F. Giustino, Origin of Superconductivity and Latent Charge Density Wave in NbS<sub>2</sub>, *Phys. Rev. Lett.* **119**, 087003 (2017).
- [55] R. Bianco, I. Errea, L. Monacelli, M. Calandra, and F. Mauri, Quantum enhancement of charge density wave in NbS<sub>2</sub> in the two-dimensional limit, *Nano Lett.* **19**, 3098 (2019).
- [56] C. D. Malliakas and M. G. Kanatzidis, Nb-Nb interactions define the charge density wave structure of 2H-NbSe<sub>2</sub>, *J. Am. Chem. Soc.* **135**, 1719 (2013).
- [57] F. Zheng and J. Feng, Electron-phonon coupling and the coexistence of superconductivity and charge-density wave in monolayer NbSe<sub>2</sub>, *Phys. Rev. B* **99**, 161119(R) (2019).
- [58] C.-S. Lian, C. Si, J. Wu, and W. Duan, First-principles study of Na-intercalated bilayer NbSe<sub>2</sub>: Suppressed charge-density wave and strain-enhanced superconductivity, *Phys. Rev. B* **96**, 235426 (2017).
- [59] A. Y. Liu, Electron-phonon coupling in compressed 1T-TaS<sub>2</sub>: Stability and superconductivity from first principles, *Phys. Rev. B* **79**, 220515(R) (2009).
- [60] Y. Ge and A. Y. Liu, First-principles investigation of the charge-density-wave instability in 1T-TaSe<sub>2</sub>, *Phys. Rev. B* **82**, 155133 (2010).
- [61] P. B. Allen and R. C. Dynes, Transition temperature of strong-coupled superconductors reanalyzed, *Phys. Rev. B* **12**, 905 (1975).
- [62] Since in bulk 2H-TX<sub>2</sub> the energy splitting of normal phase's two *d* bands crossing *E<sub>F</sub>* originates from the combined effects of interlayer interaction and spin-orbit interaction, I extract the SOC-induced splitting fraction, Δ<sub>SO</sub>, by subtracting the Fermi-surface average for the two *d* bands' energy splitting obtained without SOC from the Fermi-surface average for that obtained with SOC. The resulting lower Δ<sub>SO</sub> for the bulk does not necessarily mean weaker effects of SOC on its electron-phonon interaction and superconductivity as compared to the monolayer case, which require further theoretical demonstration.
- [63] W. L. McMillan, Transition temperature of strong-coupled superconductors, *Phys. Rev.* **167**, 331 (1968).